Rheology of granular rafts

J. Lalieu, A. Seguin, and G. Gauthier
Université Paris-Saclay, CNRS, Laboratoire FAST, F-91405 Orsay, France

(Received 25 July 2022; revised 20 October 2022; accepted 15 June 2023; published 29 June 2023)

Rheology of macroscopic particle-laden interfaces, called "granular rafts," has been experimentally studied in the simple shear configuration. The shear-stress relation obtained from a classical rheometer exhibits the same behavior as a Bingham fluid, and the viscosity diverges with the surface fraction according to evolutions similar to 2D suspensions. The velocity field of the particles that constitute the granular raft has been measured in the stationary state. These measurements reveal nonlocal rheology similar to dry granular materials. Close to the walls of the rheometer cell, one can observe regions of large local shear rate while in the middle of the cell a quasistatic zone exists. This flowing region, characteristic of granular matter, is described in the framework of an extended kinetic theory showing the evolution of the velocity profile with the imposed shear stress. Measuring the probability density functions of the instantaneous local shear rate, we provide evidence of a balance between positive and negative instantaneous local shear rate. This behavior is the signature of a quasistatic region inside the granular raft.

DOI: 10.1103/PhysRevE.107.064901

I. INTRODUCTION

Particle-laden interfaces are ubiquitous in the natural environment (e.g., insect colonies [1,2]) and industries to build materials with specific properties (e.g., electric or magnetic properties [3]), prevent sloshing [4], or stabilize foams or emulsions [5,6]. Among their intriguing behavior one can cite their ability to generate armored nonspherical or everlasting bubbles [7] which can support high over- or underpressure [8,9]. Their countless applications have generated many studies of their mechanical properties (see [10] for a review). When particles are spread on a liquid surface they deform the interface, and interaction forces between them appear. For spheres, the contact angle ζ sets the position of attachment of the liquid-air interface on the particle. For light (small Bond number [11]) and large enough particles, gravity and colloidal interactions are negligible compared to capillaries. The curvature of the interface results from the balance between the particle weight, the Archimedean force, and the capillary force which pulls the beads, leading to attractive forces between particles. Under these conditions particle-laden interfaces are often called granular rafts [12], and their ability to float, to sink, or to trap material [13,14] as well as their robustness has been widely studied [15,16]. The behavior of particle-laden interfaces under compression [17–19], or indentation [20] is fairly well understood. Their viscoelastic behavior has been studied [17,21,22], suggesting the importance of local interactions between particles in the macroscopic rheology; however, their behavior when submitted to stationary simple shear remains poorly understood.

In three dimensions, above a yield stress and in the inertial regime, dense granular materials (respectively suspensions) obey the so-called local friction constitutive law $\mu(I) = \tau/P$ [resp. $\mu(J) = \tau/P$], where τ is the shear stress and P the confining pressure, and a dilatancy law $\phi(I)$ [resp. $\phi(J)$] where ϕ is the packing fraction. μ and ϕ are scalar functions of the inertial number $I = \dot{\gamma}_\ell d/\sqrt{P/\rho}$ (resp. the viscous number $J = \eta_f \dot{\gamma}_\ell/P$), with $\dot{\gamma}_\ell$ the local shear rate, d the particle diameter, ρ their density (and η_f the fluid viscosity) [23–26]. This inertial (resp. viscous) number can be seen as the ratio between a characteristic time of strain $1/\dot{\gamma}_\ell$ and a characteristic time of rearrangement $d\sqrt{\rho/P}$ for granular matter (resp. η_f/P for suspension). However, in many cases granular materials exhibit nonlocal effects which lead to the development of a sheared region next to a quasistatic one. In these situations granular material rheology deviates from the local constitutive law, and several models have been developed to account for this nonlocality [27–33].

In order to keep the same rheological framework for the description of granular rafts, it is relevant to define a microscopic characteristic time t_c related to the rearrangement of the grains constituting the raft. For granular rafts the useful stress scale comes from the surface tension χ between the liquid and the particles which apply the confining pressure σ/d with $\sigma = \chi\cos(\zeta)$ where ζ is the contact angle. Thus the characteristic rearrangement time reads $t_c = d\sqrt{\rho d/\sigma}$, and one might build a *capillary inertial number*:

$$I_c = \frac{\dot{\gamma}_\ell d}{\sqrt{\frac{\sigma}{\rho d}}}. \tag{1}$$

Moreover, due to the curvature of the meniscus attractive capillary forces develop between particles, and granular rafts may belong to the attractive granular class of materials [34] with stronger nonlocal effects, thus different rheology.

In this paper we study the rheology of a granular raft with a classical rheometer in a double-gap cell with imposed shear stress and address the question of the locality of the particle-laden interface behavior. Granular rafts are 2D attractive granular media that exhibit a yield stress function of the particle surface fraction ϕ and whose mean behavior can be described as a Bingham fluid. When the granular raft is sheared, coupling global stress-strain measurements and displacement field measurements reveals that the local capillary inertial number I_c is not homogeneous in the rheometer cell. While accounting for this behavior by the use of a continuous hydrodynamic model based on the kinetic theory extended to dense granular systems [33,35], we highlight that in the region where I_c is smaller than a critical capillary inertial number $I_c{}^*$, the microscopic velocity fluctuations give rise to a balance between positive and negative instantaneous local shear rate, thus inhibiting the onset of a macroscopic shear. This is characteristic of a quasistatic regime and suggests a transition of the nature of the interaction between grains from a collisional regime to an elastic regime.

II. EXPERIMENTAL SETUP

Granular rafts are obtained by gently spreading silanized polystyrene spheres of diameter $d = 140$ µm and $d = 80$ µm (see Sec. VI) to probe the influence of particle size, setting the mean particle surface fraction ϕ, which is measured by direct visualization, over a mixture of water and glycerin that matches the polystyrene density so that buoyancy effects are neglected before capillary effects. Tetradecyl trimethyl ammonium bromide (TTAB) is added to the liquid phase to a concentration of 10 g L^{-1} to reduce the surface tension, and thus the cohesive force between the particles, to $\chi = 34$ mN m^{-1}, while the contact angle between the fluid and the silanized particle, measured through pendant drop method, is $\zeta \approx 80^\circ$ leading to $\sigma \approx 5.9$ mN m^{-1}. Note that 34 mN m^{-1} is the minimum value accessible with this surfactant.

Granular rafts are sheared in a homemade cylindrical double-gap cell of mean radius $R = 30$ mm whose two gaps are $e = 4.5$ mm wide, accounting for the thickness of the measuring cylinder [Fig. 1(a)]. The inside, outside, and measuring cylinders are made coarse by gluing the same particles as the ones forming the raft at their surfaces. The cell is placed into a MCR 501 rheometer (Anton Paar), and the measuring cylinder is lowered 10 mm deep into the solution. The granular raft is sheared at constant velocity $\Omega = 0.3$ Hz for 10 rotations before any measurement. The cylinder is then driven with a constant torque M, and we allow the system to flow until a steady state is achieved, with a constant rotational speed Ω_∞ measured, which comes typically in 150 s [Fig. 1(b)]. Note that the rotational speed Ω corresponds to the cylinder velocity; the actual particle velocity close to the wall may differ from Ω due to the sliding at the wall. This steady state can be achieved with both decreasing or increasing torque, showing no hysteresis or long-time variation. Due to the contribution of the fluid flow underneath the raft to the torque, a benchmark measure is performed without particles to obtain the resisting torque M_f for the pure fluid at the same rotational speed Ω_∞. We can then deduce the expression of the surface shear stress on the raft, that is, the shear stress integrated over the thickness of the raft in this double-gap configuration, to be $\tau = (M - M_f)/(4\pi R^2)$. In a fairly narrow gap configuration [$0.99 > R/(R+e) > 0.5$ [40], here $R/(R+e) \approx 0.87$], considering the mechanical equilibrium, the shear stress τ, and the pressure are homogeneous in the gap.

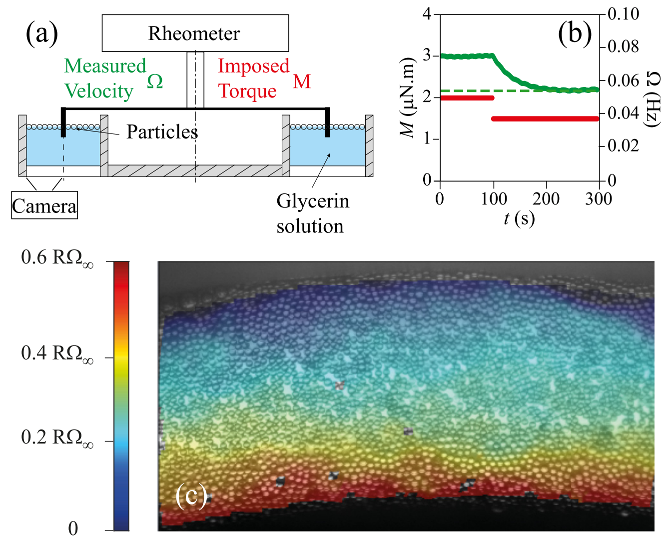

FIG. 1. (a) Sketch of the experimental setup. (b) Imposed torque $M = 1.5$ µN m (•) and measured velocity of the cylinder Ω (•) as a function of time t for $\phi = 0.74$. The dashed line represents the steady regime with $\Omega_\infty = 54$ mHz. (c) Typical instantaneous velocity field for an imposed torque $M = 6$ µN m. The color of the velocity vector represents its norm relatively to the velocity of the inner cylinder ($R\Omega_\infty = 17.5$ mm s^{-1}).

Using a camera set under the raft, we record its displacement field in the outer gap of the cell while shearing it, allowing us to detect and follow particles for a dense raft [Fig. 1(c)]. We can then process the images thus obtained via image correlation to compute the local time-averaged velocity field of the particles. Considering the flow geometry, the results will be presented in polar coordinates (r, θ) centered on the axis of the rheometer in the viewing plane of the camera [Fig. 1(c)]. Since the range of variation of r extends from R to $R + e$, we define a reduced space variable $s = (r - R)/e$ to discuss the results. Additionally, the axisymmetry of the system allows us to average spatially the results according to the orthoradial direction $\mathbf{e}_\theta$. Since no mean displacement of particles in the radial direction is observed, the instantaneous velocity field of the particles is $V_\theta(s, t)\mathbf{e}_\theta$. Averaging over time, one obtains the time-averaged velocity field $V(s) = \langle V_\theta(s, t)\rangle$. From this local velocity field, it is then possible to determine the local shear rate $\dot\gamma_\ell$. The detection of the grains is feasible in the center of the cell leading to no significant radial variations of ϕ in the range $0.3 < s < 0.9$, implying no variation in the whole gap: Sec. IV will show that for higher stresses the shear rate is homogeneous in the whole gap, leading to the conclusion that ϕ is also homogeneous. The measure of ϕ being independent of the imposed stress in the available range [Fig. 3(b)], and the number of particles being constant through the experiment, this means that ϕ is independent of the imposed stress in the whole gap and thus homogeneous.

III. RHEOMETRY

In these experiments performed in a Couette rheometer, it is usual to present the evolution of the mean (surface) stress

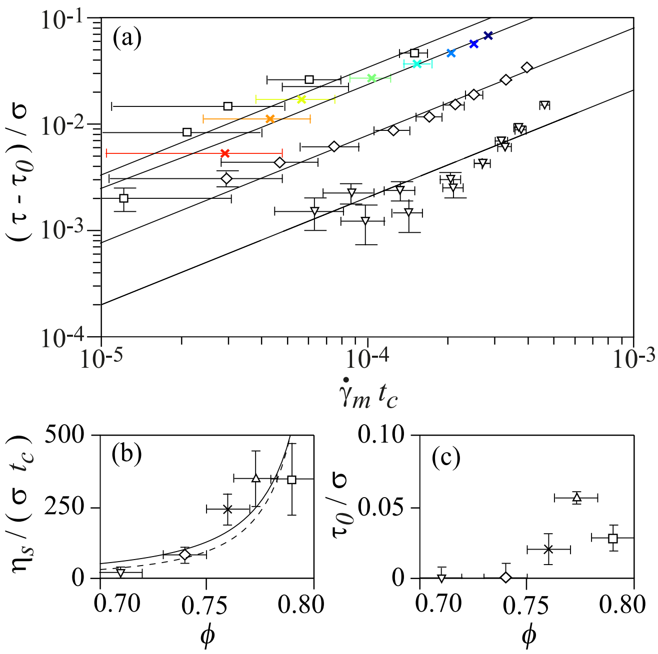

FIG. 2. (a) Dimensionless shear stress $(\tau - \tau_0)/\sigma$ as a function of the dimensionless mean strain $\dot{\gamma}_m t_c$ for different solid fractions: ($\triangledown$) $\phi = 0.71$, ($\diamond$) $\phi = 0.74$, ($\times$) $\phi = 0.76$, ($\triangle$) $\phi = 0.77$, and ($\square$) $\phi = 0.79$. The solid line represents a linear fit $\tau - \tau_0 = \eta_s(\phi)\sigma t_c \dot{\gamma}_m$ corresponding to Bingham fluid behavior. (b) Normalized surface viscosity $\eta_s/(\sigma\, t_c)$ and (c) dimensionless yield stress τ_0/σ as a function of ϕ. The solid line in (b) is given by $\eta_s/(\sigma\, t_c) = \eta_0\phi_c(\phi_c - \phi)^{-2\phi_c}$ with $\phi_c = 0.82$ and $\eta_0 = 2.83$ corresponding to the 2D suspension behavior law [36,37]. The dashed line in (b) corresponds to the Maron and Pierce law [38,39] adapted in two dimensions, $\eta_s/(\sigma\, t_c) = \eta_0\phi_c(\phi_c - \phi)^{-2}$ with $\phi_c = 0.82$ and fit parameter $\eta_0 = 0.81$.

τ as a function of the mean shear rate $\dot{\gamma}_m = R\Omega_\infty/e$ (Fig. 2). The average rheological curves show that the rheology of the granular raft follows a Bingham fluid constitutive law $\tau = \tau_0 + \eta_s\dot{\gamma}_m$ [41], where τ_0 is a 2D surface yield stress in Pa m and η_s is then a 2D surface viscosity thus expressed in Pa m s. Figure 2(a) presents the linear evolution of the normalized stress $(\tau - \tau_0)/\sigma$ as a function of the normalized shear rate $\dot{\gamma}_m t_c$ for different packing fractions ϕ. Above a critical particle surface fraction $\phi^* \approx 0.71$ granular rafts exhibit a yield stress τ_0 which increases with ϕ [Fig. 2(c)]. On either side of this critical particle surface fraction, flowing rafts do so with a constant viscosity, which is itself a growing function of ϕ [Fig. 2(b)]. The dependence of the surface viscosity η_s with the particle surface fraction ϕ is in a roughly good agreement with previous studies [17,42]. It follows the usual rheological law of 2D suspensions $\eta_s \propto (\phi_c - \phi)^{-2\phi_c}$ [36,37] showing that our setup is not singular. Note that a Maron and Pierce law used for 3D suspensions is also in reasonable agreement with our data [38,39] as shown in Fig. 2(b). Out-of-plane motion of the particles is a good candidate to explain the odd rheological behavior at very high ϕ (squares in Fig. 2). At a particle surface fraction that close to the packing fraction, a small relative change in ϕ caused by out-of-plane motion would induce a large change in the measured η_s and τ_0. We tried to check this hypothesis using a laser profilometer, unfortunately to no avail for the lack of precision of the measurement. During this experiment, the fact that the measure of ϕ for the highest stress, at the beginning of the experiment, is no noticeably different from the measure for the lowest stress, at the end of the experiment, leads to the conclusion that no significant amount of particle had sunk (<2%).

IV. VELOCITY FIELD

The images taken from a video camera are analyzed by a DIC software (DaVis, LaVision) to get the velocity field of the grains [Fig. 1(c)]. From it we extract the azimutal profile $V(s)$. In the observed range the velocity at which the cylinder rotates $R\Omega$ is never met by the grains at the wall. To account for this slip velocity, we normalize the velocity by its maximum value V_M leading to $v = V/V_M$. The values of V_M are plotted in the inset of Fig. 3(a), showing that V_M is a growing function of the imposed stress τ. However, there is no linear relation between V_M and τ, as there was when considering $\dot{\gamma}_m = R\Omega_\infty/e$, because there is no trivial proportionality between the wall velocity Ω_∞ and the velocity of the grains at the wall V_M. This once again stresses the need for a microscopic description of the flow. Figure 3(a) shows the normalized local velocity v measurements as a function of distance s from the cylinder for decreasing imposed shear stress τ. Overall, we see that the velocity decreases as the distance to the inner cylinder increases. From this velocity field, we can deduce the local shear rate $\dot{\gamma}_\ell = r\, d(V/r)/dr \simeq dV/dr$ in our experiments, within the small gap approximation. The decrease of v is rather linear when the applied stress τ is high, leading to a roughly constant shear rate $\dot{\gamma}_\ell$ in the raft. But it becomes nonlinear as τ becomes smaller. We observe a localization of the velocity close to the wall like what can be sometimes observed in dry granular media [27,35,43,44]. Thus, the local shear rate $\dot{\gamma}_\ell$ is not homogeneous, and these velocity field measurements show that the rheology of the rafts is expected to be nonlocal, different from a Newtonian fluid [45], but similar to a dry granular medium [27]. Thus the 2D Krieger-Dougherty model or Maron and Pierce law, used in Sec. III, are only true in average but cannot describe the local behavior of a granular raft.

V. HYDRODYNAMICAL MODEL

To account for nonlocality, the recent rheological models applied to granular flows define a diffusive quantity. Even though the most universal one (in its application) is the nonlocal granular fluidity (defined as $\dot{\gamma}_\ell/\mu$) [28], a recent review [46] suggests that kinetic theory can be successfully applied while also giving a microscopic physical origin for the velocity fluctuations. Thus, the kinetic theory model is both relevant and sufficient in the case of an homogeneous state of stress.

We develop a hydrodynamic model that has been used in studies around dry granular media [35,43,44,47]. The classical kinetic theory of molecular systems has been applied with some success to dilute and even dense athermal granular systems by introducing the concept of a "temperature" T related to the fluctuations of the time-averaged velocity $T(s) = \langle V_\theta(s,t)^2\rangle - V(s)^2$. Within this framework, heat is

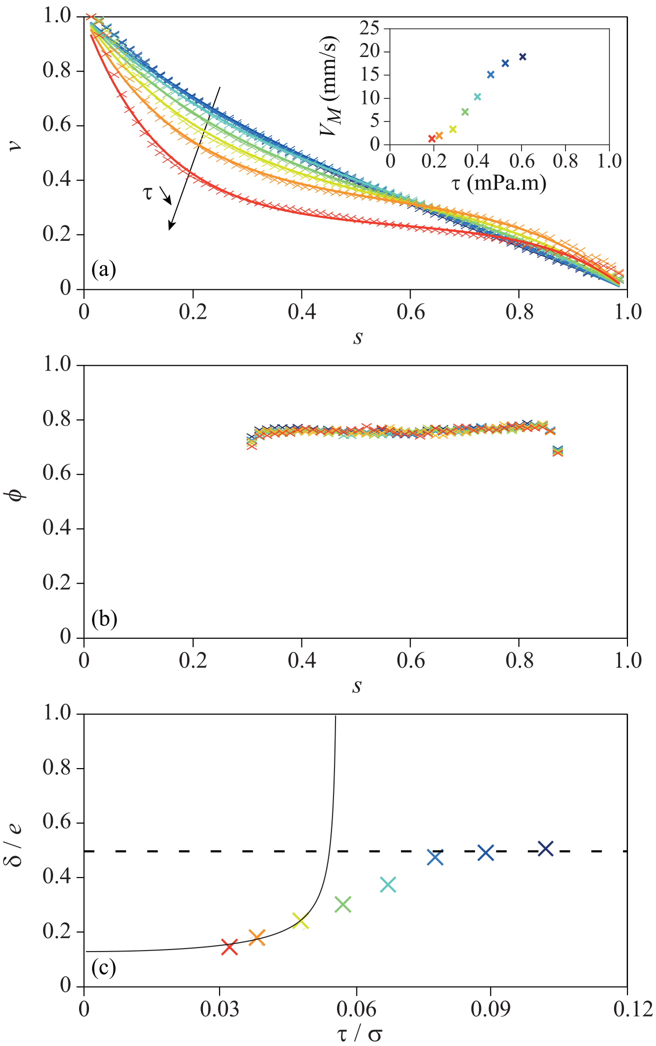

FIG. 3. (a) Normalized velocity profile v as a function of the distance s inside the gap. Same symbols and colors as in Fig. 2: the colors correspond to the value of τ. The solid lines are given by Eq. (4). Inset: Maximal velocity V_M reached at the moving wall, as a function of applied stress τ. (b) ϕ as a function of the distance s inside the gap. Same symbols and colors as in Fig. 2. (c) Characteristic length δ/e as a function of τ/σ. The solid line is obtained from the hydrodynamical model [Eq. (3)] with $(2\kappa_0\eta_0)^{1/2} = 1.9 \times 10^{-7}$ Pa m^2 and $(\epsilon_0\eta_0)^{1/2} = 3.3 \times 10^{-4}$ Pa m. The dashed line represents the saturation of the diffusion length at $\delta \approx e/2$.

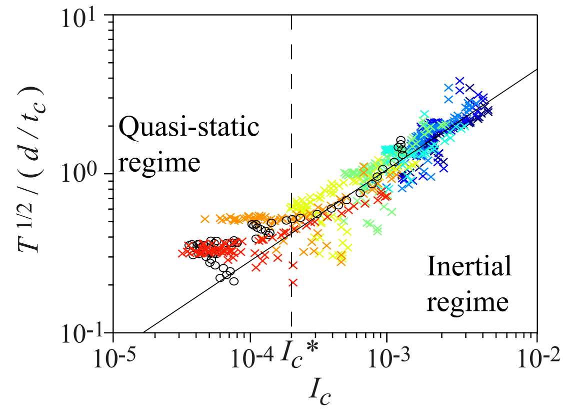

FIG. 4. Dimensionless velocity fluctuations $T^{1/2}/(d/t_c)$ as a function of I_c for different imposed τ and for $\phi = 0.76$ and $d = 140$ µm (same symbols as in Fig 2). The symbol (○) correspond to $\chi = 69$ mN m^{-1}. The solid line represents the best fit of the data $T^{1/2} \sim I_c^{1/(2\beta-1)}$ with $\beta = 1.25 \pm 0.05$.

created by the flow itself. A moving area increases locally the temperature, thus reducing the resistance to movement of the surrounding particles and allowing them to flow. This effect is then propagated until a steady state is reached. In the present case, the local velocity fluctuations are generated and exchanged in the whole raft through the contacts of the particles in the flow. Assuming pressure p and τ are homogeneous in the whole raft, the effective viscosity varies such as $\eta \propto 1/\dot{\gamma}_\ell$. In the framework of the kinetic theory of granular systems [43], one can define an effective surface viscosity η related to the temperature T such as $\eta = \eta_0 T^{-(2\beta-1)/2}$ where η_0 depends on density ρ, diameter d, mechanical properties of the particles, and the pressure p in the raft, which are constant in the experiment for a given τ, while β is a phenomenological exponent larger than or equal to unity to account for the divergence of the viscosity [35,43]. For instance, $\beta = 1$ for dilute and moderately dense system, while for a dry granular shear flow, a value of $\beta \simeq 1.75$ has been reported [35,43]. The relation between η and T implies a power law between the temperature and the local shear rate $\dot{\gamma}_\ell$. It holds in the inertial regime, that is, as long as the contacts by collisions are dominant in the dynamics of the raft; it is then useful to plot the local temperature T as a function of the local capillary inertial number I_c (Fig. 4). For high capillary inertial number I_c, Fig. 4 reveals that $T^{1/2}/(d/t_c) \sim I_c^{2/3}$. This is in agreement with kinetic theory model and leads to $\beta = 4/3$. It shows that the kinetic theory model framework is compatible with the measurements in this flowing regime. However, for low value of I_c experimental data deviate from the power law and kinetic theory is no more applied. It is then possible to define a crossover between these two regimes characterized by a critical inertial capillary number $I_c^* = 2 \times 10^{-4}$. Measures of I_c inside the raft [Fig. 5(a)] show that this criterion ($I_c > I_c^*$) is met everywhere for the higher stresses, whereas for lower applied stresses I_c is heterogeneous with a minimal value that is met at the center of the gap. This minimal value falls under the criterion $I_c < I_c^*$. Note that we do not vary d in Fig. 4. Although the complete expression is $I_c = (\tau/\eta_0)t_c T^{(2\beta-1)/2}$, the dependency of η_0 with d is not explicit since the pressure might also depend on particle diameter d. Experimentally, the measurement of the confining pressure in this 2D object remains a challenge.

As a result, only the surface tension χ can be changed without spreading the curves. We performed additional experiments without the use of surfactant in the water-glycerol mixture, thus bringing the surface tension to its highest possible value $\chi = 69$ mN m^{-1} (which has been measured using pendant drop method), with a surface fraction of $\phi = 0.77$ that should be close enough to the previous one ($\phi = 0.76$) to allow for comparison. In our framework this should lead to a change in the proposed scaling, with $t_c' \simeq t_c/\sqrt{2}$. We plot the result of this experiment in Fig. 4, superposing the two experiments, to check the

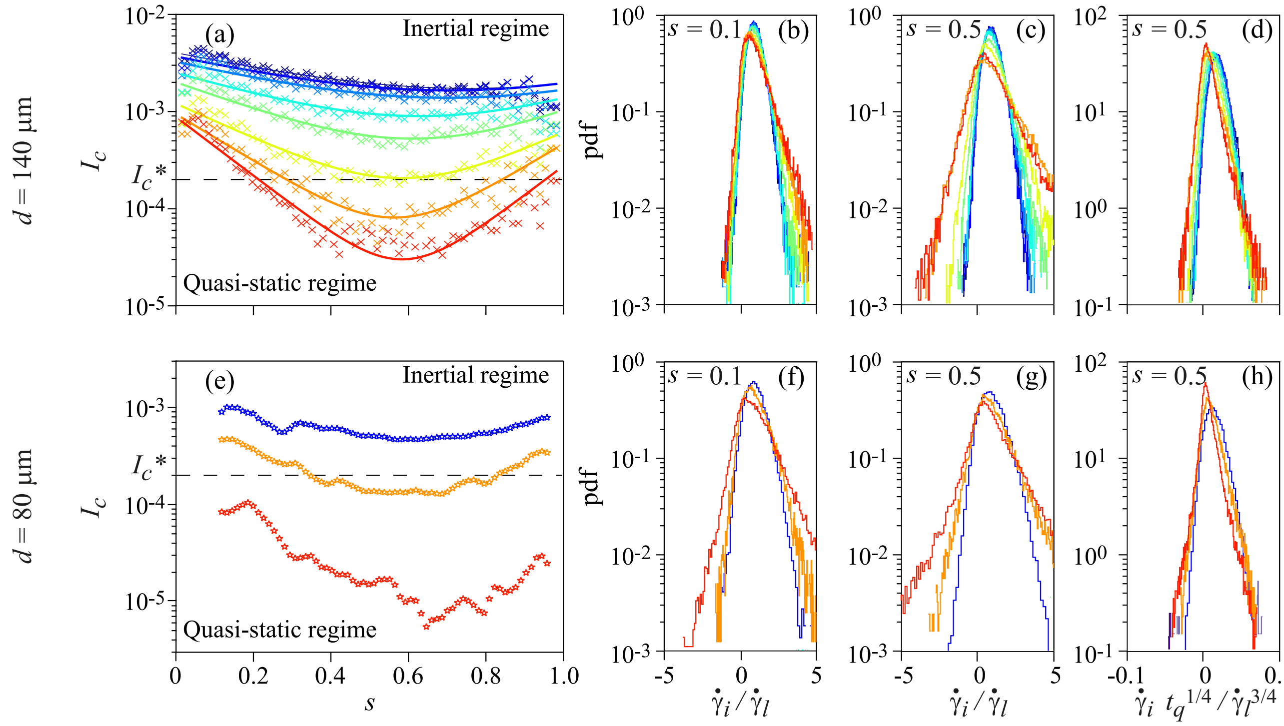

FIG. 5. (a) I_c as a function of s. The dashed line represents the critical value I_c^* delimiting the two flow regimes. PDF of instantaneous local shear rate $\dot{\gamma}_i$ normalized: by the mean local strain $\dot{\gamma}_\ell$ in the flowing region (b) and quasistatic region (c) and by $\dot{\gamma}_\ell^{3/4}$ in the quasistatic region (d). Same colors as in Fig. 3(a). (e) I_c as a function of s for different imposed stress (☆) $\tau/\sigma = 0.014$, (☆) $\tau/\sigma = 0.022$, (☆) $\tau/\sigma = 0.041$ and for $\phi = 0.76$ and $d = 80$ μm. The dashed line represents the critical value I_c^* delimiting the two flow regimes. PDF of instantaneous local shear rate $\dot{\gamma}_i$ normalized by the mean local strain $\dot{\gamma}_\ell$ in the flowing region (f) and quasistatic region (g) and by $\dot{\gamma}_\ell^{3/4}$ in the quasistatic region (h).

validity of the scaling in defining the criterion I_c^*. Even though the factor $\sqrt{2}$ in the scaling has a noticeable effect, this is not incompatible with the other experiments (Fig. 4).

Above I_c^*, the temperature obeys the heat equation, and to obtain an analytical solution while introducing no noticeable error (given the range of variation of $T^{1/2}$), we set $\beta = 1$ leading to $I_c = \dot{\gamma}_\ell t_c = \tau T^{1/2} t_c/\eta_0$. In our 2D configuration, the heat equation is an equilibrium between diffusion (with a transport coefficient reducing to $\kappa = \kappa_0 T^{-1/2}$), collision dissipation (with a dissipation coefficient reducing to $\varepsilon = \varepsilon_0 T^{-1/2}$), and source term corresponding to $\tau\dot{\gamma}_\ell$. κ_0 and ε_0 depend on density, diameter, and mechanical properties of the grains and pressure p, which are constant in our case. In our geometry the hydrodynamic equation for $T(s)$ comes down to

$$\frac{d}{ds}\left(\kappa(T)\frac{dT}{ds}\right) - \varepsilon(T)T + \frac{\tau^2}{\eta_0}T^{1/2} = 0, \qquad (2)$$

which can be integrated to obtain

$$\frac{d^3 v}{ds^3} - \frac{1}{\delta^2}\frac{dv}{ds} = 0, \qquad (3)$$

where $\delta = [(2\kappa_0\eta_0)/(\varepsilon_0\eta_0 - \tau^2)]^{1/2}$ is a characteristic length. Solving Eq. (3) using $v(0) = 1$ and $v(1) = 0$ gives

$$v(s) = A\left[\cosh\left(\frac{(2s-1)e}{2\delta}\right) - \cosh\left(\frac{e}{2\delta}\right)\right] + \exp\left(-\frac{se}{2\delta}\right)\frac{\sinh\left(\frac{(1-s)e}{2\delta}\right)}{\sinh\left(\frac{e}{2\delta}\right)} \qquad (4)$$

with A a fitting parameter. This analytical function has been fitted on the velocity profiles showing an excellent agreement with the experimental data [Fig. 3(a)]. Note that the velocity profile so obtained presumes that the whole raft is in an inertial regime: while this is not true, the contribution of the quasistatic regime in the overall macroscopic dynamics of the flow is too small to be noticed. These fits are robust and can be derived in order to extend them to the I_c profiles [Fig. 5(a)]. The diffusion length δ, which is found in the analytical solution for v, is a growing function of τ, as observed in Fig. 3(c). Its evolution differs, however, from the analytical model. For the higher imposed stress, the shear rate is uniform in the cell's gap and δ reaches a maximal value, $\delta \approx e/2$ dashed line in Fig. 3(c)]. The model predicts, for an infinite system, a divergence of the diffusion length for a maximal stress $(\epsilon_0\eta_0)^{1/2}$. The saturation of the diffusion length experimentally recorded may be imputed to the Newtonian fluid that flows under the raft, which tends to impose a uniform shear. The diffusion length saturates due to the finite size of the cell and the stress continues to grow over the maximal value deduced from the fit in Fig. 3(c) $(\epsilon_0\eta_0)^{1/2}/\sigma = 0.056$.

VI. QUASISTATIC REGIME

Despite the good agreement between the velocity profiles deduced from Eq. (4) and the experimental data, below the critical inertial capillary number I_c^* the system is no longer described with the hydrodynamical model (left flat parts of the curves in Fig. 4). The remaining dynamics of the raft for $I_c < I_c^*$ is then not contact driven but may be forced by the flow underneath, allowing for nonzero velocities in an otherwise quasistatic regime as proposed by numerical studies [33,48,49]. According to them, for $I_c(s) < I_c^*$, the system is in a quasistatic regime (similar to a plug flow) in which the strain and thus the velocity fluctuations are sustained by the boundary conditions. In this regime instantaneous local shear rate $\dot{\gamma}_i$, defined as $dV(r,t)/dr$, occurs over time in and against the forcing. The probability density functions (PDFs) of instantaneous local shear rate $\dot{\gamma}_i$ normalized with the time-averaged local shear rate $\dot{\gamma}_l$ for two radial locations $s = 0.1$ and $s = 0.5$ are displayed in Figs. 5(b) and 5(c). For $s = 0.1$, $I_c > I_c^*$ for any $\tau > \tau_0$, the raft is in a flowing regime, the PDFs are narrow, and the instantaneous local shear rate is positive, i.e., in the direction of $\dot{\gamma}_\ell$ [Fig. 5(b)]. This is in agreement with a predominance of a viscous component of the stress (due to particle collisions), over an elastic one, as developed in another numerical study [50]: as particles are freely flowing against one another, the stress τ and $\dot{\gamma}_\ell$ are proportional, and the energy input is $\tau\dot{\gamma}_\ell$ and balances with the viscous dissipation, which is proportional to $\dot{\gamma}_i^2$ in a rearrangement event. At $s = 0.5$, for the higher imposed torques ($\tau/\sigma \geqslant 5.7 \times 10^{-2}$), $I_c > I_c^*$ and the PDFs are similar: they are narrow and the instantaneous local shear rate all positive. It is no more the case at lower imposed torques ($\tau/\sigma \leqslant 4.7 \times 10^{-2}$), for which $I_c \leqslant I_c^*$: the PDFs are broad and present negative values; the lower the capillary inertial number is the broader the distribution. For the lowest imposed torque [$\tau/\sigma = 3.2 \times 10^{-2}$, red curve in Fig. 5(c)], the PDF displays comparable proportions of positive and negative instantaneous local shear rate. These instantaneous local shear rates opposed to the shear flow are characteristic of the quasistatic regime [33]. The fact that PDFs do not rescale with $\dot{\gamma}_\ell$ but with $\dot{\gamma}_\ell^{3/4}$ [Fig. 5(d)] is another sign of the different dynamics at play. Based on numerical work [50] relying on the Durian foam bubble model [51], the shift in scaling tends to demonstrate the predominance of an elastic component in the stress in this regime, where elastic energy is released with rare, sudden, and significant rearrangements. During these events, particles need to overcome an exceeding stress, similar to a microscopic yield stress, to put in motion their surroundings. As a result, the model predicts that $\tau \sim \dot{\gamma}_\ell^{1/2}$ and the energy production goes as $\dot{\gamma}_\ell^{3/2}$ [50]. The viscous dissipation still being in $\dot{\gamma}_i^2$, the PDF should rescale with $\dot{\gamma}_\ell^{3/4}$. The elastic energy loss is balanced by the viscous dissipation with a characteristic time $t_q = \eta d/\sigma$. While the velocity profiles cannot show it, the PDFs of Figs. 5(b)–5(d) highlight that the quasistatic regime corresponds to this elastoplastic regime.

Would the kinetic theory model apply on the whole gap, the microscopic dynamics should be homogeneous. Consequently, the PDFs should follow the same scaling as $\dot{\gamma}_i/\dot{\gamma}_\ell$. The experiment shows that this is not true. However, the difference between the experimental data and the model provided by the kinetic theory is of the order of 10^{-5} on the values of I_c [Fig. 5(a)]. This difference, once integrated on the velocity profiles, does not create major differences on the whole profile [Fig. 3(a)].

To account for the dependence of I_c with the particle diameter d, we performed experiments with $d = 80$ μm with results in agreement with the suggested scalings [Figs. 5(e)–5(h)]. The I_c profiles are displayed on Fig. 5(e), and their general shape is the same as for $d = 140$ μm. The velocity profiles follow a similar trend, and the shear rate can be either heterogeneous or homogeneous depending on the applied stress. For the lowest stress $\tau/\sigma = 0.014$, I_c is inhomogeneous and is always below I_c^*. For the highest stress $\tau/\sigma = 0.041$, I_c is always above I_c^*. This is confirmed by the PDF scalings of the instantaneous local shear rate: for $s = 0.1$ the two PDF that rescale with $\dot{\gamma}_\ell$ are the ones corresponding to I_c above I_c^* [Fig. 5(f)], while for $s = 0.5$ the PDFs do not rescale with $\dot{\gamma}_\ell$ but with $\dot{\gamma}_\ell^{3/4}$ [Figs. 5(f) and 5(h)].

VII. CONCLUSION

The mechanical behavior of granular rafts is close to the one of attractive granular materials. Below a yield stress τ_0 the material is static, and no local fluctuations of the particle position are measurable. As for granular materials and above the yield stress, the flow exhibits a nonuniform shear, thus revealing two flow regimes that are characterized by a local capillary inertial number I_c [Eq. (1)]. A hydrodynamical model developed from kinetic theory describes well the flow, and as predicted by a recent numerical model [33], below the critical value I_c^* the system is in a quasistatic regime. The signature of this quasistatic regime is reflected in the scalings of the probability density function of the instantaneous local shear rate $\dot{\gamma}_i$, as proposed by another numerical model [50]. This suggests that the macroscopic transition in the flow regime is in agreement with a microscopic transition in the nature of contacts between the particles. The critical value $I_c^* \approx 2 \times 10^{-4}$ is found to be one order of magnitude lower than the one predicted for 2D cohesion-free granular materials $I^* \approx 5 \times 10^{-3}$, in agreement with numerical study which reported that characteristic relaxation time t_c can be two orders of magnitude lower for attractive granular materials [52]. When the behavior of the granular raft is described by an hydrodynamical model, the diffusion length δ increases with the shear stress τ, though because of the presence of the Newtonian fluid under the raft and the finite size of the cell δ it cannot be larger than half the gap of the cell.

ACKNOWLEDGMENTS

We are grateful to L. Auffray, J. Amarni, A. Aubertin, C. Manquest, and R. Pidoux for the development of the experimental setup. The authors thank N. Retailleau, Y. Khidas, O. Pitois, X. Chateau, V. Langlois, and F. Rouyer for fruitful discussions. This work is supported by the project PhyGaMa ANR-19-CE30-0009-02.

[1] J. C. Loudet, A. M. Alsayed, J. Zhang, and A. G. Yodh, Phys. Rev. Lett. **94**, 018301 (2005).
[2] N. J. Mlot, C. A. Tovey, and D. L. Hu, Proc. Natl. Acad. Sci. USA **108**, 7669 (2011).
[3] J. Forth, P. Y. Kim, G. Xie, X. Liu, B. A. Helms, and T. P. Russell, Adv. Mater. **31**, 1806370 (2019).
[4] F. Moisy, J. Bouvard, and W. Herreman, Europhys. Lett. **122**, 34002 (2018).
[5] S. U. Pickering, J. Chem. Soc., Trans. **91**, 2001 (1907).
[6] B. P. Binks and R. Murakami, Nat. Mater. **5**, 865 (2006).
[7] A. Roux, A. Duchesne, and M. Baudoin, Phys. Rev. Fluids **7**, L011601 (2022).
[8] A. Bala Subramaniam, M. Abkarian, L. Mahadevan, and H. A. Stone, Nature (London) **438**, 930 (2005).
[9] Y. Timounay, O. Pitois, and F. Rouyer, Phys. Rev. Lett. **118**, 228001 (2017).
[10] O. Pitois and F. Rouyer, Curr. Opin. Colloid Interface Sci. **43**, 125 (2019).
[11] D. Vella and L. Mahadevan, Am. J. Phys. **73**, 817 (2005).
[12] P. Cicuta and D. Vella, Phys. Rev. Lett. **102**, 138302 (2009).
[13] S. Protière, C. Josserand, J. M. Aristoff, H. A. Stone, and M. Abkarian, Phys. Rev. Lett. **118**, 108001 (2017).
[14] A. Lagarde and S. Protière, Phys. Rev. Fluids **5**, 044003 (2020).
[15] P. Petit, A.-L. Biance, E. Lorenceau, and C. Planchette, Phys. Rev. E **93**, 042802 (2016).
[16] C. Planchette, E. Lorenceau, and A.-L. Biance, Soft Matter **14**, 6419 (2018).
[17] D. Zang, E. Rio, D. Langevin, B. Wei, and B. Binks, Eur. Phys. J. E **31**, 125 (2010).
[18] E. Jambon-Puillet, C. Josserand, and S. Protiere, Phys. Rev. Mater. **1**, 042601(R) (2017).
[19] O. Saavedra V., H. Elettro, and F. Melo, Phys. Rev. Mater. **2**, 043603 (2018).
[20] W. He, Y. Sun, and A. D. Dinsmore, Soft Matter **16**, 2497 (2020).
[21] S. Barman and G. F. Christopher, Langmuir **30**, 9752 (2014).
[22] S. Barman and G. F. Christopher, J. Rheol. **60**, 35 (2016).
[23] GDR MiDi, Eur. Phys. J. E **14**, 341 (2004).
[24] C. Cassar, M. Nicolas, and O. Pouliquen, Phys. Fluids **17**, 103301 (2005).
[25] P. Jop, Y. Forterre, and O. Pouliquen, Nature (London) **441**, 727 (2006).
[26] F. Boyer, É. Guazzelli, and O. Pouliquen, Phys. Rev. Lett. **107**, 188301 (2011).
[27] K. A. Reddy, Y. Forterre, and O. Pouliquen, Phys. Rev. Lett. **106**, 108301 (2011).
[28] L. Bocquet, A. Colin, and A. Ajdari, Phys. Rev. Lett. **103**, 036001 (2009).
[29] M. Bouzid, M. Trulsson, P. Claudin, E. Clément, and B. Andréotti, Phys. Rev. Lett. **111**, 238301 (2013).
[30] M. Bouzid, A. Izzet, M. Trulsson, E. Clément, P. Claudin, and B. Andreotti, Eur. Phys. J. E **38**, 125 (2015).
[31] D. L. Henann and K. Kamrin, Phys. Rev. Lett. **113**, 178001 (2014).
[32] A. Thomas, Z. Tang, K. E. Daniels, and N. Vriend, Soft Matter **15**, 8532 (2019).
[33] J. Gaume, G. Chambon, and M. Naaim, Phys. Rev. Lett. **125**, 188001 (2020).
[34] G. Lois, J. Blawzdziewicz, and C. S. O'Hern, Phys. Rev. Lett. **100**, 028001 (2008).
[35] W. Losert, L. Bocquet, T. C. Lubensky, and J. P. Gollub, Phys. Rev. Lett. **85**, 1428 (2000).
[36] I. M. Krieger, Adv. Colloids Interface Sci. **3**, 111 (1972).
[37] J. F. Brady, Int. J. Multiphase Flow **10**, 113 (1983).
[38] S. H. Maron and P. E. Pierce, J. Colloid Sci. **11**, 80 (1956).
[39] É. Guazzelli and O. Pouliquen, J. Fluid Mech. **852**, P1 (2018).
[40] C. W. Macosko, *Measurements and Applications* (Wiley, VCH Publishes, 1994).
[41] E. C. Bingham, Rheology principles, measurements and applications, *Fluidity and Plasticity* (McGraw-Hill, New York, 1922), Vol. 2.
[42] S. Reynaert, P. Moldenaers, and J. Vermant, Phys. Chem. Chem. Phys. **9**, 6463 (2007).
[43] L. Bocquet, W. Losert, D. Schalk, T. C. Lubensky, and J. P. Gollub, Phys. Rev. E **65**, 011307 (2001).
[44] A. Seguin, Y. Bertho, P. Gondret, and J. Crassous, Phys. Rev. Lett. **107**, 048001 (2011).
[45] E. Guyon, J.-P. Hulin, L. Petit, and C. D. Mitescu, *Physical Hydrodynamics* (Oxford University Press, Oxford, 2001).
[46] K. Kamrin, Front. Phys. **7**, 116 (2019).
[47] A. Seguin and P. Gondret, Phys. Rev. E **96**, 032905 (2017).
[48] S. Khamseh, J.-N. Roux, and F. Chevoir, Phys. Rev. E **92**, 022201 (2015).
[49] G. Koval, J.-N. Roux, A. Corfdir, and F. Chevoir, Phys. Rev. E **79**, 021306 (2009).
[50] B. P. Tighe, E. Woldhuis, J. J. C. Remmers, W. van Saarloos, and M. van Hecke, Phys. Rev. Lett. **105**, 088303 (2010).
[51] D. J. Durian, Phys. Rev. Lett. **75**, 4780 (1995).
[52] P. Chaudhuri, L. Berthier, and L. Bocquet, Phys. Rev. E **85**, 021503 (2012).